J Physiol 593.3 (2015) pp 521–539

The Journal of Physiology

TECHNIQUES FOR PHYSIOLOGY

Photoreleasable ligands to study intracrine angiotensin II signalling

Artavazd Tadevosyan[1,2], Myriam Létourneau[3,4], Benjamin Folch[3], Nicolas Doucet[4,5,6], Louis R. Villeneuve[2], Aida M. Mamarbachi[2], Darlaine Pétrin[7], Terence E. Hébert[7], Alain Fournier[3,4], David Chatenet[3,4], Bruce G. Allen[1,2,7,8] and Stanley Nattel[1,2,7]

[1] *Department of Medicine, Université de Montréal, Montréal, Québec, Canada*
[2] *Montreal Heart Institute, Montréal, Québec, Canada*
[3] *INRS–Institut Armand-Frappier, Université du Québec, Québec, Canada*
[4] *Laboratoire international associé Samuel de Champlain-INSERM/U982 and INRS-Institut Armand-Frappier*
[5] *PROTEO, Québec Network for Research on Protein Function, Structure, and Engineering, Université Laval, Laval, Québec, Canada*
[6] *Groupe de Recherche Axé sur la Structure des Protéines, McGill University, Montréal, Québec, Canada*
[7] *Department of Pharmacology and Therapeutics, McGill University, Montréal, Québec, Canada*
[8] *Department of Biochemistry and Molecular Medicine, Université de Montréal, Montréal, Québec, Canada*

Key points

- The renin–angiotensin system plays a key role in cardiovascular physiology and its over-activation has been implicated in the pathogenesis of several major cardiovascular diseases.
- There is growing evidence that angiotensin II (Ang-II) may function as an intracellular peptide to activate intracellular/nuclear receptors and their downstream signalling effectors independently of cell surface receptors.
- Current methods used to study intracrine Ang-II signalling are limited to indirect approaches because of a lack of selective intracellularly-acting probes.
- Here, we present novel photoreleasable Ang-II analogues used to probe intracellular actions with spatial and temporal precision.
- The photorelease of intracellular Ang-II causes nuclear and cytosolic calcium mobilization and initiates the de novo synthesis of RNA in cardiac cells, demonstrating the application of the method.

Abstract Several lines of evidence suggest that intracellular angiotensin II (Ang-II) contributes to the regulation of cardiac contractility, renal salt reabsorption, vascular tone and metabolism; however, work on intracrine Ang-II signalling has been limited to indirect approaches because of a lack of selective intracellularly-acting probes. Here, we aimed to synthesize and characterize cell-permeant Ang-II analogues that are inactive without uncaging, but release active Ang-II upon exposure to a flash of UV-light, and act as novel tools for use in the study of intracrine Ang-II physiology. We prepared three novel caged Ang-II analogues, [Tyr(DMNB)^4]Ang-II, Ang-II-ODMNB and [Tyr(DMNB)^4]Ang-II-ODMNB, based upon the incorporation of the photolabile moiety 4,5-dimethoxy-2-nitrobenzyl (DMNB). Compared to Ang-II, the caged Ang-II analogues showed 2–3 orders of magnitude reduced affinity toward both angiotensin type-1 (AT1R) and type-2 (AT2R) receptors in competition binding assays, and greatly-reduced potency in contraction assays of rat thoracic aorta. After receiving UV-irradiation, all three caged Ang-II analogues released Ang-II and potently induced the contraction of rat thoracic aorta. [Tyr(DMNB)^4]Ang-II showed the most rapid photolysis upon UV-irradiation and was the focus of subsequent characterization. Whereas Ang-II and photolysed [Tyr(DMNB)^4]Ang-II increased ERK1/2 phosphorylation (via AT1R) and cGMP production (AT2R), caged [Tyr(DMNB)^4]Ang-II did not. Cellular uptake of [Tyr(DMNB)^4]Ang-II was 4-fold greater than that of Ang-II and

DOI: 10.1113/jphysiol.2014.279109

significantly greater than uptake driven by the positive-control HIV TAT(48–60) peptide. Intracellular photolysis of [Tyr(DMNB)^4]Ang-II induced an increase in nucleoplasmic Ca^{2+} ($[Ca^{2+}]_n$), and initiated 18S rRNA and nuclear factor kappa B mRNA synthesis in adult cardiac cells. We conclude that caged Ang-II analogues represent powerful new tools for use in the selective study of intracrine signalling via Ang-II.

(Received 11 June 2014; accepted after revision 20 November 2014; first published online 26 November 2014)
Corresponding author S. Nattel or B. G. Allen: 5000 Bélanger Street, Montréal, Québec, H1T 1C8, Canada. Email: bruce.g.allen@umontreal.ca or stanley.nattel@icm-mhi.org

Abbreviations Ang-II, angiotensin II; 2-APB, 2-aminoethoxydiphenylborate; AT1R, angiotensin type-1 receptor; AT2R, angiotensin type-2 receptor; BOP, benzotriazol-1-yl-oxy-tris(dimethylamino)phosphonium hexafluorophosphate; DCM, methylene chloride; DMEM, Dulbecco's modified Eagle's medium; DMF, *N*,*N*-dimethylformamide; DMNB, 4,5-dimethoxy-2-nitrobenzyl; ECFP, enhanced cyan fluorescent protein; ERK, extracellular signal regulated kinase; HEK 293, human embryonic kidney 293; IP_3, inositol trisphosphate; NF-κB, nuclear factor kappa B; RAS, renin–angiotensin system; RP, reverse phase; TFA, trifluoroacetic acid.

Introduction

The renin–angiotensin system (RAS) is critically involved in controlling functions at various levels, from cells to tissues to the entire organism. The physiological actions of RAS and its blockade have been translated into clinical settings, improving both the quality and duration of life for patients with hypertension, heart failure, renal insufficiency, myocardial infarction and stroke (Kobori *et al.* 2007; Lang & Struthers, 2013). RAS activation is initiated after cleavage of angiotensinogen into angiotensin-I (Ang-I) via renin synthesized in juxtaglomerular cells of renal afferent arterioles. Subsequently, angiotensin-converting enzyme hydrolyses the inactive decapeptide Ang-I into the biologically active octapeptide angiotensin-II (Ang-II), which exerts actions via heterotrimeric G protein-coupled type-1 (AT1R) and type-2 (AT2R) receptors.

Although the RAS has been traditionally viewed as an endocrine system, a variety of studies point to the intracellular ('intracrine') actions of Ang-II. Angiotensin receptors are localized on the nuclear envelope of numerous cell types (Robertson & Khairallah, 1971; Haller *et al.* 1999; Cook *et al.* 2006). Exposure of isolated cardiac nuclei to Ang-II causes inositol 1,4,5-trisphosphate (IP_3)-dependent Ca^{2+}-release and *de novo* RNA synthesis (Tadevosyan *et al.* 2010, 2012). Hyperglycaemia stimulates local Ang-II production in the hearts of diabetic patients and is implicated in the increased expression of transforming growth factor-β and collagen (Frustaci *et al.* 2000; Singh *et al.* 2008). The intracrine actions attributed to Ang-II are not prevented by acute extracellular application of angiotensin receptor blockers or angiotensin-converting enzyme inhibitors (Tadevosyan *et al.* 2010). Because these compounds have a limited capacity to cross the plasma membrane, they are unable to abolish the cytosolic synthesis of Ang-II or its binding to cognate receptors on the nuclear membrane (Schwab *et al.* 1990; Singh *et al.* 2007). A direct demonstration of the intracrine effects of Ang-II has been hampered because of difficulty in selectively targeting intracellular Ang-II receptors without activating cell-surface receptors; therefore, the role of intracellular Ang-II signalling in mediating the effects of RAS activation remains poorly understood.

Better spatial and temporal resolution of biologically active molecules can be achieved with the use of 'caged compounds', characterized by the addition of a photolabile group on a substituent essential for receptor recognition (Yu *et al.* 2010). This approach has been used to study cellularly localized actions of a range of molecules, including ATP (McCray *et al.* 1980), GTP (Schlichting *et al.* 1989), endothelin-1, (Bourgault *et al.* 2007; Merlen *et al.* 2013), isoproterenol (Muralidharan & Nerbonne, 1995; Vaniotis *et al.* 2013), phenylephrine (Muralidharan *et al.* 1993), γ-aminobutyric acid (Wang & Augustine, 1995), urotensin II (Bourgault *et al.* 2005), endothelin receptor antagonists (Merlen *et al.* 2013), IP_3 (Li *et al.* 1998; Tertyshnikova & Fein, 1998), cofilin (Ghosh *et al.* 2004), DNA (Monroe *et al.* 1999) and RNA (Chaulk & MacMillan, 1998; Ando *et al.* 2001). Caged molecules can be introduced non-invasively into the cell in an inert form and then subsequently uncaged with a focused pulse of UV-light, allowing downstream effects to be monitored without disrupting other aspects of the system (Merlen *et al.* 2013; Vaniotis *et al.* 2013), which is a feature that is not exhibited by conventional reagents.

Ang-II displays stringent conformational and dynamic requirements for the amino acids at position 4 (tyrosine) and 8 (phenylalanine) for receptor binding (Aumelas *et al.* 1985; Samanen *et al.* 1989; Bovy *et al.* 1990; Noda *et al.* 1995). Ang-II analogues bearing modifications at positions 4 or 8 differentially activate post-receptor signalling in a biased fashion, and thus give rise to distinct biological outcomes (Zimmerman *et al.* 2012). To develop a tool with which to study the consequences of the selective

activation of intracellular Ang-II receptors, we synthesized photo-activatable caged analogues of Ang-II by adding a photolabile 4,5-dimethoxy-2-nitrobenzyl (DMNB) residue on the phenolic group of tyrosine-4 and/or on the α-COOH of phenylalanine 8, thereby creating three 'caged' analogues of Ang-II: [Tyr(DMNB)^4]Ang-II, Ang-II-ODMNB and [Tyr(DMNB)^4]Ang-II-ODMNB. Here, we report for the first time the design, synthesis and characterization of these compounds that can be photolysed to release Ang-II. We go on to show that photo-activated [Tyr(DMNB)^4]Ang-II demonstrates intracrine regulation of cardiomyocyte nuclear calcium content and gene expression.

Methods

Cell culture and AT1R/AT2R transfection

Human embryonic kidney 293 (HEK 293) cells were cultured in Dulbecco's modified Eagle's medium (DMEM) supplemented with 10% fetal bovine serum, 100 μg ml^{-1} streptomycin, 100 units ml^{-1} penicillin, and 2 mM L-glutamine at 37°C in a humidified atmosphere containing 5% CO_2. HEK 293 cells were seeded at a density of 4×10^4 cells per 20 mm well of 24-well plates, 1×10^5 cells per 35 mm well of 6-well plates, or 10^6 cells per 100 mm culture dish. For transient expression in HEK 293 cells, expression vectors encoding AT1R-Venus or AT2R-Venus were transfected into cells with polyethylenimine at a final concentration of 9 μg ml^{-1} (Zhang *et al.* 2009). Radioligand binding assays, immunoblots, or enzyme-linked immunosorbent assay experiments were carried out 48 h after transfection.

Synthesis and purification of caged Ang-II analogues

All Ang-II analogues were synthesized manually on a 2-chlorotrityl chloride resin (0.7 mmol g^{-1}) using solid-phase peptide synthesis with Fmoc chemistry. Synthesis of Fmoc-Tyr(DMNB)-OH was performed as described previously (Bourgault *et al.* 2005, 2007). Coupling of protected amino acids, monitored with the qualitative ninhydrin-test, was performed with a 3-equivalent excess of the protected amino acids, based on the original substitution of the resins, benzotriazol-1-yl-oxy-tris(dimethylamino)phosphonium hexafluorophosphate (BOP; 3 equiv) and *N,N*-diisopropylethylamine (6 equiv) in *N,N*-dimethylformamide (DMF) for 45 min. Fmoc removal was achieved with 20% piperidine in DMF for 20 min. After deprotection, the resin was washed extensively with DMF (1×), methanol (1×), methylene chloride (DCM) (1×) and DMF (2×) before starting another cycle for the introduction of the next amino acid. Cleavage of Ang-II and [Tyr(DMNB)^4]-Ang-II from the resin was performed with a mixture of trifluoroacetic acid (TFA)/triisopropylsilane/phenol/water (92/2.5/3/2.5) for 2 h. After evaporation of the solvent, the crude peptides were precipitated by addition of cold diethyl ether. The products were isolated, dissolved in water and freeze-dried. For C-terminally modified peptides Ang-II-ODMNB and [Tyr(DMNB)^4]-Ang-II-ODMNB, cleavage from the solid support was carried out with AcOH/trifluoroethanol/DCM (1:1:8; v/v/v) to produce fully protected peptides with a free carboxy-terminal function. The C-terminal carboxylic acid was reacted with DMNB alcohol, as described previously (Bourgault *et al.* 2007) C-terminally caged Ang-II analogues were obtained by stirring the protected peptides bearing a C-terminal DMNB ester group with TFA/triisopropylsilane/phenol/water (92/2.5/3/2.5). Similarly, to obtain fluorescein-conjugated peptides, a N-protected ε-amino acid spacer (Fmoc-aminohexanoic acid-OH) was coupled to peptidyl-resins using the BOP reagent condensation methodology (see above). After Fmoc removal, the free amino group was allowed to react overnight with fluorescein isothiocyanate (1.2 equiv) in a DMF/DCM mixture (1:1), in presence of triethylamine (20 equiv) (Jullian *et al.* 2009). TFA cleavage (TFA/triisopropylsilane/phenol/water; 92/2.5/3/2.5; 2 h) produced the expected fluorescent peptides. Crude peptides were purified by preparative reverse phase (RP)-HPLC using a C_{18} column (Phenomenex, Torrance, CA, USA) (300 Å pore size, 15 μm bead diameter, 250 mm × 21.2 mm) at a flow rate of 20 mL min^{-1}. Peptides were eluted with a linear gradient of 0–100% solution B over 2 h (solution A: 0.06% TFA/H_2O, solution B: 40% CH_3CN in 0.06% TFA/H_2O). The absorbance was monitored at 229 nm. To confirm the purity and mass of the purified products, aliquots of the collected fractions were (i) resolved by analytical RP-HPLC using a CSC-Kromasil C_{18} column (100 Å pore size, 5 μm bead diameter, 250 mm × 4.6 mm) connected to a Beckman 128 pump and Beckman 168 PDA detector (Beckman Coulter, Fullerton, CA, USA), at a flow rate of 1 ml min^{-1}, and (ii) assessed by matrix-assisted laser desorption ionization-time of flight mass spectrometry (Voyager DE system; Applied Biosystems, Foster City, CA, USA). Fractions from preparative HPLC found to have the expected m/z value and >95% pure were pooled, lyophilized and stored at −20°C.

Competition binding assays

Purified Ang-II (10 μg) was radiolabelled with Na^{125}I (0.3 mCi) using chloramine-T (5 μg) in 0.05 M phosphate buffer (pH 7.4) at room temperature for 60 s. The reaction was stopped by addition of 10 mM sodium metabisulfite and then applied to a Sep-Pak C_{18} cartridge (Waters Corp., Milford, MA, USA).

[^{125}I]Ang-II was eluted with a 60% CH_3CN/H_20 0.1% TFA solution and stored at −20°C until use. Competition binding assays employed concentrations of unlabelled ligands (Ang-II, [Tyr(DMNB)^4]Ang-II, Ang-II-ODMNB, [Tyr(DMNB)^4]Ang-II-ODMNB) ranging from 10^{-10} M to 10^{-5} M. HEK 293 cells transfected transiently with AT1R-Venus or AT2R-Venus were seeded in 24-well plates, gently washed twice with PBS and incubated for 45 min at 37°C in binding buffer (DMEM, 0.1% BSA) containing [^{125}I]Ang-II (50,000 cpm well^{-1}) plus the indicated concentrations of unlabelled ligand. At the end of the incubation period, buffer was removed by suction and cells were washed twice with ice-cold PBS, before being treated with 0.5 M NaOH for 10 min at room temperature (Bosnyak *et al.* 2011). The material in each well, corresponding to bound radioligand, was quantified using a Wallac Wizard 1470 γ-counter (Wallac Oy, Turku, Finland). Non-specific binding was measured in the presence of 1 μM unlabelled Ang-II. The statistical fit of the data with one- or two-site models was initially evaluated with Akaike's information criteria and extra sum-of-squares *F* test comparisons of model fits, and both AT1 and AT2 data were best fitted by a single-site binding model. To determine the pIC_{50} values for each Ang-II analogue, data were fit to a one-site model by non-linear regression using Graphpad Prism, version 6.0c (GraphPad Software, La Jolla, CA, USA).

Preparation of rat thoracic aortic rings and measurement of contraction strength

Aortic rings were prepared from male Sprague–Dawley rats (250–300 g) killed by CO_2 asphyxiation. All animal care and handling procedures were performed in accordance with the Canadian Council for the Care of Laboratory Animals and were approved by the Institutional Animal Research Ethics Committee, Institut National de la Recherche Scientifique – Institut Armand-Frappier and by the Montreal Heart Institute. The descending thoracic aorta was excised, transferred to a Petri dish containing Krebs bicarbonate buffer (118.4 mM NaCl, 4.7 mM KCl, 2.5 mM $CaCl_2$, 1.2 mM KH_2PO_4, 1.2 mM $MgSO_4$, 25 mM $NaHCO_3$, 11 mM glucose, pH 7.4) and cleaned of connective tissue. The endothelium was removed from aortic rings by gently rubbing the luminal surface and the vessel was cut into 4 mm rings. Single aortic rings were mounted in 5 ml organ baths (37°C) filled with Krebs solution aerated with carbogen gas (95% O_2, 5% CO_2). Isometric force-displacement transducers connected to a Grass 7E polygraph (Grass Instrument, Quincy, MA, USA) were used to measure changes in contraction. Aortic rings were allowed to equilibrate for 1 h under a resting tension of 1 g with buffer changes every 15 min. Once the tension was stable, a reference contractile response was obtained by stimulating with 40 mM KCl. Aortic rings were then washed multiple times, and the contractile response to Ang-II or the caged Ang-II analogues was determined using cumulative concentration–response curves. For each ring preparation, the contractile response was expressed as a percentage of the change in tension induced by 40 mM KCl.

Extracellular signal regulated kinase (ERK)1/2 phosphorylation

HEK 293 cells seeded in uncoated 6-well plates were transfected with either AT1R-Venus or AT2R-Venus as described above. Cells were serum-starved for 24 h prior to stimulation. On the day of the experiment, cells were washed twice with serum-free DMEM and the assay was initiated by adding the indicated ligands and incubated at 37°C. To terminate the incubation, cells were placed on ice, the medium was removed, and then cells were washed twice with ice-cold PBS. They were then scraped into ice-cold lysis buffer [25 mM Na-Hepes (pH 7.4), 150 mM NaCl, 25 mM NaF, 10 mM $MgCl_2$, 1 mM EGTA, 1 mM Na_3VO_4, 0.025% sodium deoxycholate, 10% glycerol (v/v), 10 μg ml^{-1} leupeptin, 10 μM benzamidine, 0.5 μM microcystin, 1% Triton X-100 (v/v), 0.1 mM phenylmethylsulfonyl fluoride and 5 mM dithiothreitol]. After a 30 min incubation on ice, lysates were cleared by centrifugation at 10,000 *g* for 10 min, and the supernatants retained. The protein concentration of each lysate was determined, before being denatured using Laemmli sample buffer, and resolved by SDS-PAGE (precast 10% acrylamide gels; Bio-Rad Laboratories, Hercules, CA, USA). Proteins were transferred onto polyvinylidene difluoride membranes, probed with a phospho-ERK1/2-specific antibody (Cell Signaling Technology, Beverly, MA, USA) and then, after stripping the membranes with Re-blot Plus mild antibody stripping solution (Millipore), re-probed using an ERK1/2-specific antibody (Abcam, Cambridge, MA, USA) to assess the total ERK immunoreactivity. Horseradish peroxidase-conjugated secondary antibodies (Jackson ImmunoResearch, West Grove, PA, USA) were used and immunoreactive bands were revealed by chemiluminescence and quantified using the Quantity One 1-D analysis software (Bio-Rad Laboratories).

Assessment of angiotensin receptor expression in thoracic aorta

HEK 293 cells, HEK 293-AT1R, HEK 293-AT2R or an isolated thoracic aorta were lysed by homogenizing samples in cold 300 mM sucrose, 60 mM KCl, 0.5 mM EGTA, 2 mM EDTA, 1 mM dithiothreitol, 1 mM $MgCl_2 \cdot 6H_2O$, 50 mM Hepes, 20 mM NaF, 0.2 mM Na_3VO_4, 20 mM β-glycerophosphate, 0.5 mM 4-(2-aminoethyl) benzenesulfonyl fluoride hydrochloride, 25 μg ml^{-1}

leupeptin, 10 μg ml^{-1} aprotinin, 1 μg ml^{-1} pepstatin, 1 μM microcystin and 0.1% NP40 (pH 7.4). Samples were then sonicated with two 10 s pulses, and intact cells, nuclei and cell debris were removed by centrifugation (500 *g* for 10 min). The supernatant was centrifuged (80000 *g* for 60 min) to pellet the membrane fraction, the supernatants discarded and 50 μg of each membrane fraction was resolved on SDS-PAGE. After transfer, membranes were probed with AT1R (Alomone Labs, Jerusalem, Israel), AT2R (Alomone Labs) or *N*-cadherin (BD Biosciences, Palo Alto, CA, USA) specific antibodies.

Live-cell fluorescence imaging

To assess the cell permeability of [Tyr(DMNB)^4]Ang-II, fluorescein-conjugated derivatives of Ang-II, [Tyr(DMNB)^4]Ang-II, TAT(48–60) and PACAP(28–38) were synthesized and the accumulation of fluorescein-conjugated peptides in HEK 293 cells was examined. HEK 293 cells (non-transfected) were grown on glass coverslips, incubated for 60 min at 37°C with the fluorescent peptide in Hepes–Krebs–Ringer solution buffer (5 mM Hepes, 2.68 mM KCl, 137 mM NaCl, 2.05 mM $MgCl_2$, 1.8 mM $CaCl_2$ and 1 g l^{-1} glucose, pH 7.4), washed extensively, and then incubated for 5 min with Cell Mask (dilution 1:1000; Invitrogen, Carlsbad, CA, USA) and DRAQ5 (dilution 1:1000; BioStatus, Shepshed, UK) to label the plasma membrane and nucleus, respectively. Fluorescence was then visualized with a FluoView FV1000 inverted confocal microscope (Olympus, Tokyo, Japan). Separate channels were employed for each fluorophore (i.e. fluorescein isothiocyanate, Cell Mask, DRAQ5) and the emission channels scanned sequentially to minimize cross-talk between overlapping emission spectra. Cells were imaged by serial z-stack progressive scans, background fluorescence subtracted, and fluorescence values quantified using FluoView Software (FV10-ASW).

To visualize changes in nucleoplasmic Ca^{2+} concentration ($[Ca^{2+}]_n$), freshly isolated canine ventricular cardiomyocytes were plated at 37°C for 60 min on laminin-coated 35 mm glass bottom culture dishes in Tyrode's physiological buffer. Cells were loaded with 5 μM Fluo-4AM (Invitrogen; from a 2.5 mM Fluo-4AM/10% Pluronic F125/DMSO stock) for 30 min in 10 mM Hepes (pH 7.4), 134 mM NaCl, 6 mM KCl, 10 mM glucose, 2 mM $CaCl_2$, 1 mM $MgCl_2$, and in the absence or presence of [Tyr(DMNB)^4]Ang-II, as described previously (Merlen *et al.* 2013). Cardiomyocytes were washed three times, stained with a live-cell-permeant DNA dye (DRAQ5; 1 μM) and used for Ca^{2+} imaging within 1 h. Images were obtained using a LSM 7 Duo microscope (combined LSM710 and Zeiss Live systems) (Carl Zeiss, Oberkochen, Germany) with a 63×/1.4 oil Plan-Apochromat objective. Fluo-4AM was excited using a 488 nm/100 mW diode (1–5% laser intensity) and fluorescence emitted between 495 nm and 550 nm was collected. Cells were scanned at 30 fps in bi-directional mode. The pixel size was set at 0.2 μm and the pinhole at 1.5 Airy units. After establishing a baseline, [Tyr(DMNB)^4]Ang-II was photolysed by a 70 μW pulse of UV-light using a 405-nm/30 mW diode. The power output from the 405-nm diode was measured at the level of the stage using an EC Plan-Neofluar (Carl Zeiss) 10×/0.3 objective lens with an X-Cite XR2100 optical power measurement system (Lumen Dynamics Group Inc., Mississauga, ON, Canada). DRAQ5 emissions were used to focus the UV-laser into a 60 μm^2 rectangular region overlapping the nucleus. The microscope stage (Observer Z1; Carl Zeiss) was equipped with a BC 405/561 dichroic mirror that permitted simultaneous photolysis of [Tyr(DMNB)^4]Ang-II (LSM 710 405 nm laser) and image acquisition (Zeiss Live). Intranuclear Ca^{2+} levels were expressed as a percentage of fluorescence intensity relative to basal fluorescence ($\Delta[Ca^{2+}]$Nuc(F/F$_0$;%)); basal fluorescence is the fluorescence intensity acquired 1 s prior to uncaging the [Tyr(DMNB)^4]Ang-II.

Flow cytometry

Uptake of peptides into HEK 293 cells was quantified by flow cytometry. HEK 293 cells were incubated for 60 min at 37°C in the presence of the fluorescein-conjugated derivatives of Ang-II, [Tyr(DMNB)^4]Ang-II, TAT(48–60) or PACAP(28–38) in Hepes–Krebs–Ringer solution buffer. After multiple washes with an isotonic acidic aqueous solution (200 mM glycine, 100 mM NaCl, pH 4.0) and PBS to remove extracellular fluorescein-peptides, cells were detached by trypsinization, centrifuged at 1000 *g* for 5 min, and resuspended in PBS. To identify non-viable cells, propidium iodide (0.5 μg ml^{-1}) was added prior to analysis. A minimum of 10,000 viable cells per sample were analysed using a FACScan system (Becton Dickinson, Franklin Lakes, NJ, USA). The mean fluorescence intensity of the live cell population was used for further analysis using FlowJo software (Tree Star Inc., Ashland, OR, USA).

Canine cardiomyocyte isolation

Cardiac cell isolation was performed by perfusion with Tyrode's solution containing collagenase (100 U ml^{-1}; Worthington, type II) as described previously (Tadevosyan *et al.* 2015).

Quantitative PCR

RNA from cardiac cells was extracted with Trizol (Life Technologies, Grand Island, NY, USA) in accordance with the manufacturer's instructions. cDNA was synthesized from 1 μg RNA with the use of a High Capacity cDNA Reverse Transcription Kit (Applied Biosystems).

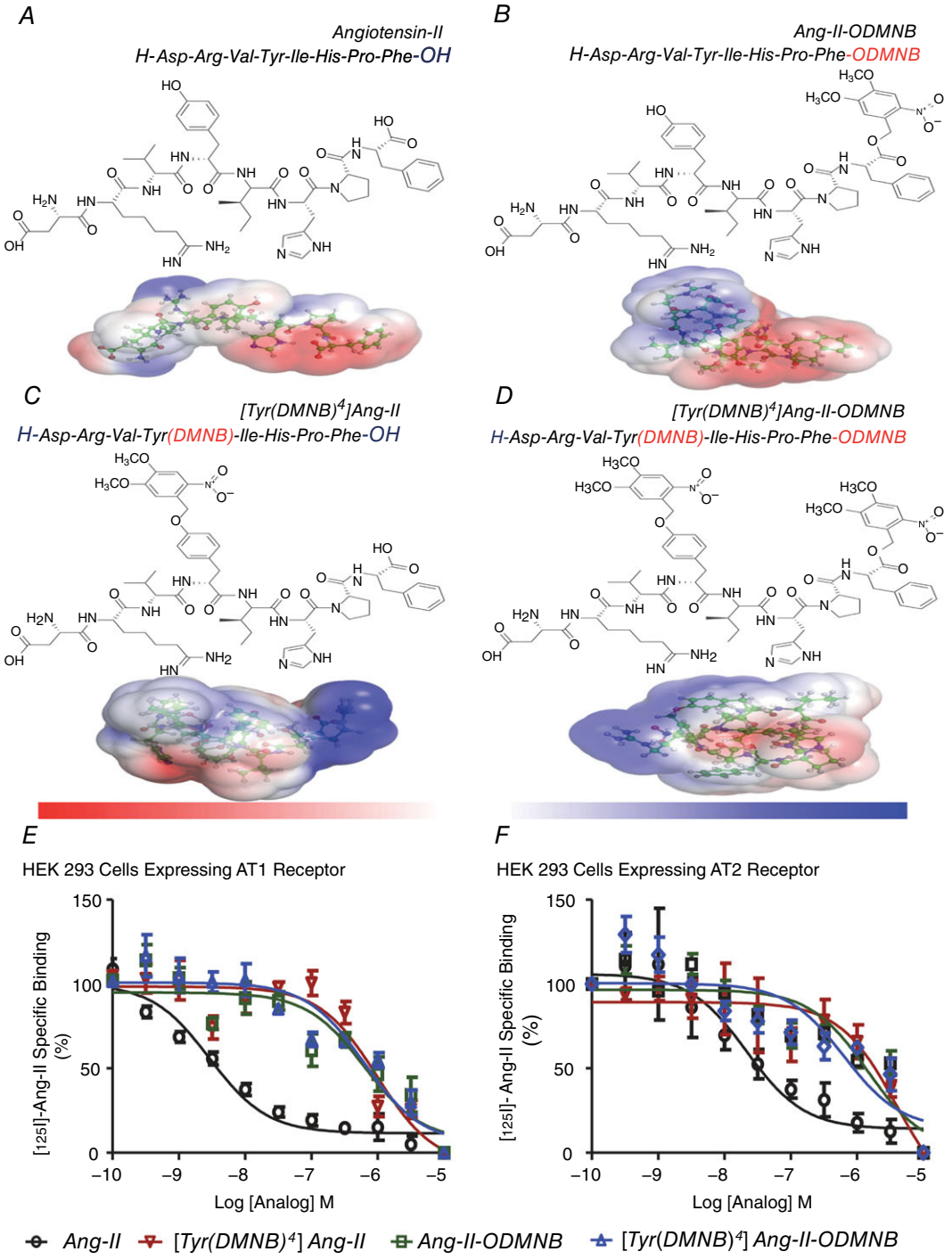

Figure 1. Structures of the caged Ang-II analogues and competitive displacement of [^{125}I]Ang-II by caged Ang-II analogues
A, Ang-II. *B*, Ang-II-ODMNB. *C*, [Tyr(DMNB)^4]Ang-II. *D*, [Tyr(DMNB)^4]Ang-II-ODMNB. The position of the photosensitive DMNB moiety is indicated in brackets and was added either on the side chain of the tyrosine at position 4, the C-terminal carboxylic function of phenylalanine-8, or at both sites. Red and blue surfaces describe negative and positive electrostatic potentials (-3.5 k_BT, $+3.5$ k_BT), respectively. Three-dimensional structures were generated using PyMol visualization software. The electrostatic potentials were calculated using the Adaptive Poisson-Boltzmann Solver with the PyMol tool. (*E*, *F*, competitive displacement of [^{125}I]Ang-II by Ang-II or caged Ang-II analogues (n = 6/condition) in HEK 293 cells transfected with AT1R or AT2R. Data are percentage of specific radioligand binding in absence of competitors. Non-specific binding was determined in the presence of 1 μM Ang-II.

Table 1. Physicochemical and binding properties of Ang-II and its photolabile analogues, as evaluated by competition binding assays using HEK 293-AT1 and HEK 293-AT2 transfected cells

Compound Name	MS^{calc} (g mol^{-1})*	$^{b}MS^{found}$ (g mol^{-1})†	Purity‡	Binding ^{125}I-Ang-II (HEK293-AT1R)			Binding ^{125}I-Ang-II (HEK293-AT2R)		
				IC_{50} (nM)	pIC_{50}	*n*	IC_{50} (nM)	pIC_{50}	*n*
Ang-II	1046.18	1047.10	≥95%	3.2	8.58 ± 0.10	8	32	7.65 ± 0.18	6
[Tyr(DMNB)^4]Ang-II	1241.35	1241.52	≥95%	1110	6.01 ± 0.11	6	1640	6.88 ± 0.61	6
Ang-II-ODMNB	1241.35	1242.43	≥95%	915	6.13 ± 0.27	6	470	6.45 ± 0.28	5
[Tyr(DMNB)^4]Ang-II-ODMNB	1436.52	1437.52	≥95%	1140	6.31 ± 0.27	6	1930	6.54 ± 0.52	6

*Theoretical monoisotopic molecular weight as calculated with ChemDraw Ultra, version 7.0.1 (Perkin Elmer, Boston, MA, USA). †*m/z* value assessed by matrix-assisted laser desorption ionization-time of flight mass spectrometry. ‡Percentage of purity determined by HPLC using the eluent system: A = H_2O containing 0.06% TFA and B = 40% CH_3CN in aqueous 0.06% TFA, with a gradient of 1% B min^{-1} and a flow rate of 1 ml min^{-1} on a Jupiter C_{18} column (Phenomenex). Detection at 229 nm.

Quantitative PCR assays were performed as described previously (Dawson *et al.* 2012) using TaqMan probes and primers (Applied Biosystems): eukaryotic 18S rRNA (Assay ID: Hs03003631_g1), nuclear factor kappa B (NFkB) (Assay ID: Cf02622547_m1) and HPRT1 (Assay ID: Cf02626255_g1). HPRT1 was used as an internal standard. Each RNA was assessed in duplicate and analysed with the ΔC_t method.

Statistical analysis

Data from radioligand binding and functional assays were obtained from a minimum of 3 independent experiments and are presented as the mean ± SEM. EC_{50}, pEC_{50}, IC_{50} and pIC_{50} values were determined by fitting experimental data by non-linear regression with GraphPad Prism, version 6.0c. Student's t test (for single 2-group comparisons), as well as one-way or two-way ANOVA with Bonferroni *post hoc* tests (multiple groups with a common control), were used for statistical comparisons. $P < 0.05$ was considered statistically significant.

Results

Design and synthesis of photo-activable caged Ang-II analogues

Previous structure–function studies have shown that Ang-II activates AT1 and AT2 receptors through an induced-fit mechanism; for which the aromatic Tyr^4 moiety and the α-COOH group of Phe^8 are crucial for biological activity (Aumelas *et al.* 1985; Bovy *et al.* 1990; Noda *et al.* 1995; Samanen *et al.* 1989) Accordingly, we designed and synthesized three Ang-II analogues incorporating the photolabile nitrobenzyl substituent, DMNB, on either the phenolic function of Tyr^4, the terminal α-COOH group, or both (Fig. 1*A*–*D*). The caging substituent was stable when exposed to (i) 20% piperidine in DMF during removal of the Fmoc N-protecting group and (ii) 100% TFA during peptide cleavage from the resin used in solid phase synthesis. Each Ang-II analogue eluted from RP-HPLC as a single major product. The purity of each fraction was assessed and confirmed by analytical HPLC. Analysis of Ang-II, [Tyr(DMNB)^4]Ang-II, Ang-II-ODMNB and [Tyr(DMNB)^4]Ang-II-ODMNB by mass spectrometry revealed a major peak corresponding to the calculated molecular mass (Table 1). Computational structural analysis using PyMol molecular visualization software (http://www.pymol.org) predicted that the addition of the DMNB group induces conformational changes, including alterations in both main chain torsion angles and side chain orientation (Fig. 1*A*–*D*).

For use in the study of intracrine Ang-II signalling in intact cells, a caged Ang-II analogue must possess certain characteristics (relative to unmodified Ang-II): (i) reduced affinity for ATR1 and ATR2 binding; (ii) reduced affinity and efficacy for ATR1 and ATR2 activation; (iii) rapid uncaging without inducing cell damage and release of the original unmodified form of the ligand upon uncaging; (iv) increased cell permeability; and (v) physiological activity of the intracellular form under conditions in which extracellular activation is excluded. Below, a characterization of [Tyr(DMNB)^4]Ang-II, Ang-II-ODMNB and [Tyr(DMNB)^4]Ang-II-ODMNB is provided according to these criteria.

Pharmacological characterization of the caged Ang-II analogues

Radioligand binding assays showed a strong rightward shift in the displacement curve for all three analogues compared to Ang-II (Fig. 1*E* and *F*). The shift indicated between 100- and 1000-fold reduced binding affinity. Unmodified Ang-II displaced [^{125}I]Ang-II binding to AT1R or AT2R with IC_{50} values of 3.2 nM and 32 nM,

respectively. By contrast, the caged analogues displaced [^{125}I]Ang-II with much higher IC_{50} values, indicating affinity reductions of 2–3 orders of magnitude: for AT1R and AT2R, respectively: [Tyr(DMNB)^4]Ang-II, 1.1 μM and 1.6 μM; Ang-II-ODMNB, 0.91 μM and 0.47 μM; [Tyr(DMNB)^4]Ang-II-ODMNB, 1.1 μM and 1.9 μM (Table 1).

The ability of the caged Ang-II analogues (in the absence of uncaging) to activate cell-surface angiotensin receptors was evaluated by concentration–response curve bioassays using rat thoracic aortic ring preparations (Fig. 2*A*–*D*), which expresses both AT1R and AT2R (Fig. 2*E*). Ang-II evoked a concentration-dependent contraction with a pEC_{50} of 8.10 ± 0.15 and a maximal efficacy (E_{max}) of 134% ± 11% ($n = 7$). All caged Ang-II analogues were far less potent than Ang-II (Fig. 2*F*) and induced no detectable vasoconstriction at concentrations of the order (10^{-8} M) used to study intracrine signalling.

Photorelease kinetics and action of caged Ang-II analogues

Photorelease kinetics of the caged Ang-II analogues (10^{-8} M) upon exposure to UV-light were examined by mass spectrometry (Fig. 3*A*–*C*). UV-irradiation (100 W) caused a time-dependent decrease in the abundance of each caged Ang-II analogue (indicating its photolysis), with a concomitant increase in free Ang-II (corresponding to Ang-II release via cleavage of the photolabile group). Mass spectrometry revealed that no significant side reactions releasing products other than Ang-II occurred during photolysis. Of the three caged Ang-II analogues, [Tyr(DMNB)^4]Ang-II showed the fastest rate of release (Fig. 3*D*). The time-course of changes in concentration of the caged compound ([Tyr(DMNB)^4]Ang-II) and the free Ang-II product of photolysis was confirmed independently with 3 different

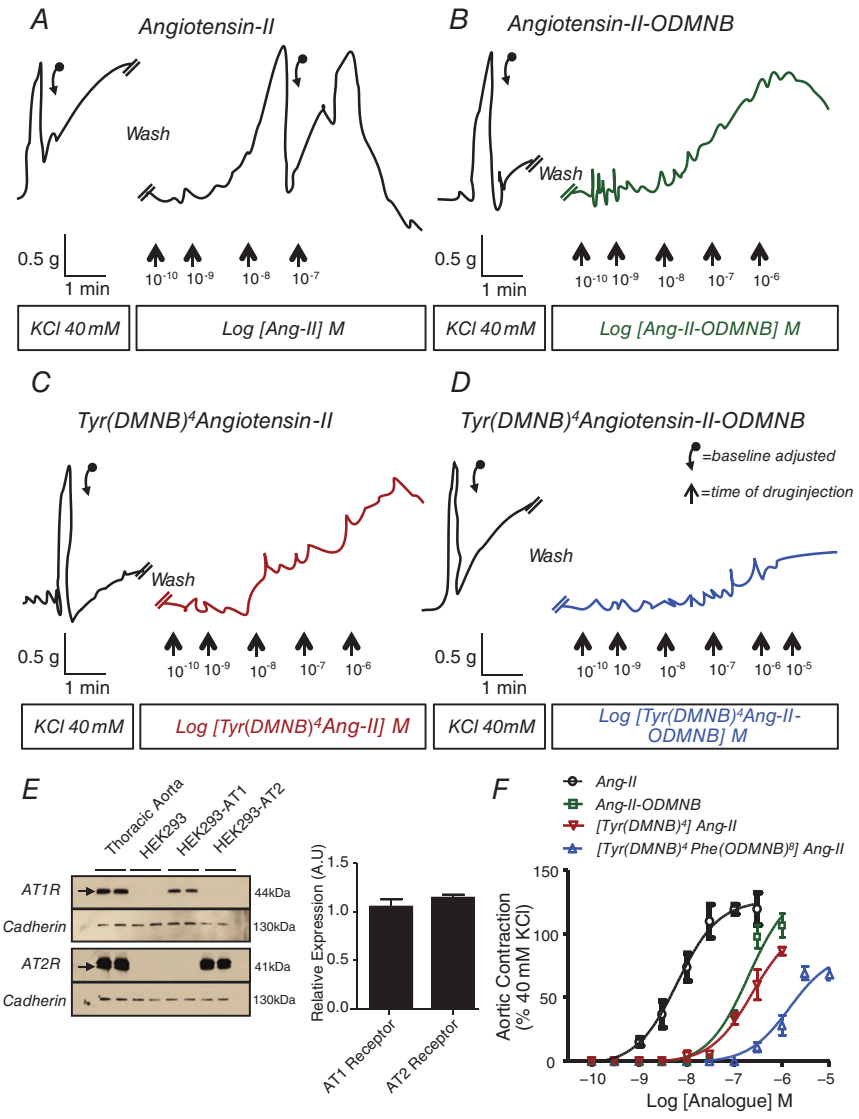

Figure 2. Concentration-dependent responses of rat thoracic aortic rings to various analogues without uncaging
Contraction-recordings were obtained with a curvilinear pen recorder for (*A*) Ang-II, (*B*) Ang-II-ODMNB, (*C*) [Tyr(DMNB)^4]Ang-II and (*D*) [Tyr(DMNB)^4]Ang-II-DMNB. *E*, immunoblotting for AT1R, AT2R and *N*-cadherin (positive control) in membranes isolated from rat thoracic aorta, as well as HEK 293, HEK 293-AT1R and HEK 293-AT2R cells. *F*, overall results expressed as percentage of contractile response induced by 40 mM KCl. Data are shown as the mean ± SEM of at least 5 experiments per group performed on tissues isolated from separate animals for each experiment. Descending arrows on original recordings indicate baseline adjustment.

UV-exposure durations (1 s, 1 min and 3 min) by HPLC (Fig. 3*E*).

We next sought to verify that photolysis resulted in the release of physiologically functional Ang-II. After assessing their contractile response to 40 mM KCl as a reference, we incubated aortic rings with caged Ang-II analogues at concentrations (10^{-8} M) that were inactive in the absence of photolysis, and then photolysis was induced by UV-irradiation at the same time as monitoring tension. UV-irradiation in the absence of caged Ang-II did not increase tension (Fig. 4*A*). By contrast, in the presence of the caged compounds, UV-irradiation induced time-dependent increases in tension of aortic ring preparations, after an initial ~2–3 min delay. The rate of rise of the tension varied among the compounds (note differences in time-scales of Fig. 4*B–D*). Photolysis of [Tyr(DMNB)^4]Ang-II induced the fastest-rising response (Fig. 4*B–D*). Figure 4*E* shows a quantification of the response from its onset for each probe, with the results expressed as percentage of maximal 40 mM KCl-response (mean ± SEM values for all experiments with each agent). The fastest appearing response was clearly seen with [Tyr(DMNB)^4]Ang-II, consistent with its rapid uncaging rate in Fig. 3*D*. Thus, the caged Ang-II analogues described here show a very limited ability to bind to and activate ATRs in the absence of photolysis; upon photolysis, they release pharmacologically active Ang-II. Because [Tyr(DMNB)^4]Ang-II displayed minimal intrinsic activity, rapid photolysis and clear biological activity after UV-irradiation, we focused on the evaluation of [Tyr(DMNB)^4]Ang-II for further study of intracrine Ang-II signalling in live cells.

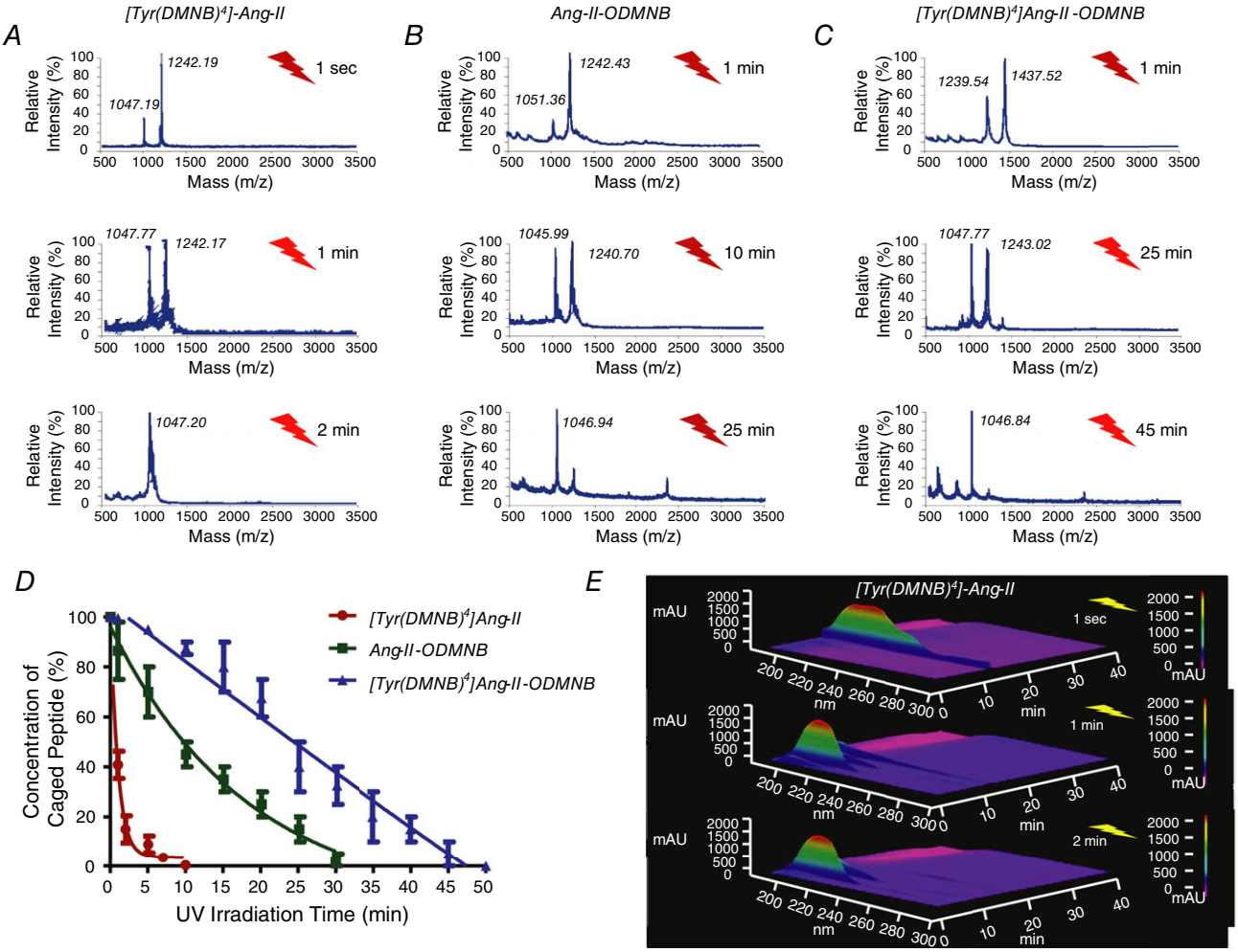

Figure 3. Photolysis kinetics of various analogues
Photolysis (100-W UV-lamp) of a 10^{-8} M solution of (*A*) [Tyr(DMNB)^4]Ang-II, (*B*) Ang-II-ODMNB and (*C*) [Tyr(DMNB)^4]Ang-II-ODMNB was performed in Krebs–Henseleit buffer and analysed by mass spectrometry ($n = 3$ per group). *D*, caged peptide concentration over time after UV-irradiation. *E*, signal-intensity (*Y*-axis) *versus* wavelength (*X*-axis) and HPLC elution-time (*Z*-axis) at different times after photorelease of [Tyr(DMNB)^4]Ang-II as analysed by analytical HPLC.

Photolysis of [Tyr(DMNB)^4]Ang-II activates AT1R-mediated ERK signalling

To further investigate the biological activity of Ang-II photoreleased from caged analogues, we examined an AT1R-specific response to extracellular Ang-II. ERK1/2 is activated by mitogenic signals, including AT1R-stimulation. Accordingly, we examined the effects of extracellular [Tyr(DMNB)^4]Ang-II and Ang-II via AT1R activation by assessing ERK1/2 phosphorylation in HEK 293 cells transiently transfected with AT1R. Ang-II (5 min for 37°C) increased ERK phosphorylation in a concentration-dependent manner that was half-maximal at $\sim 10^{-8}$ M (Fig. 5*A*). At a concentration as high as 10^{-6} M, [Tyr(DMNB)^4]Ang-II did not induce ERK1/2 phosphorylation in the absence of photolysis (Fig. 5*B*). By contrast, upon photolysis [Tyr(DMNB)^4]Ang-II induced a concentration-dependent increase in ERK1/2 phosphorylation (Fig. 5*C*), with a maximum level of ERK1/2 phosphorylation similar to Ang-II (Fig. 5*D*). Consistent with AT1R-mediated ERK activation in HEK 293 cells, Ang-II-induced ERK phosphorylation was inhibited by AT1R blockade with valsartan (Fig. 5*E* and *F*). UV-irradiation alone did not increase ERK1/2 phosphorylation. Hence, [Tyr(DMNB)^4]Ang-II is unable to activate AT1R-induced ERK-phosphorylation at concentrations as high as 1 μM, but shows full pharmacological activity upon photolysis.

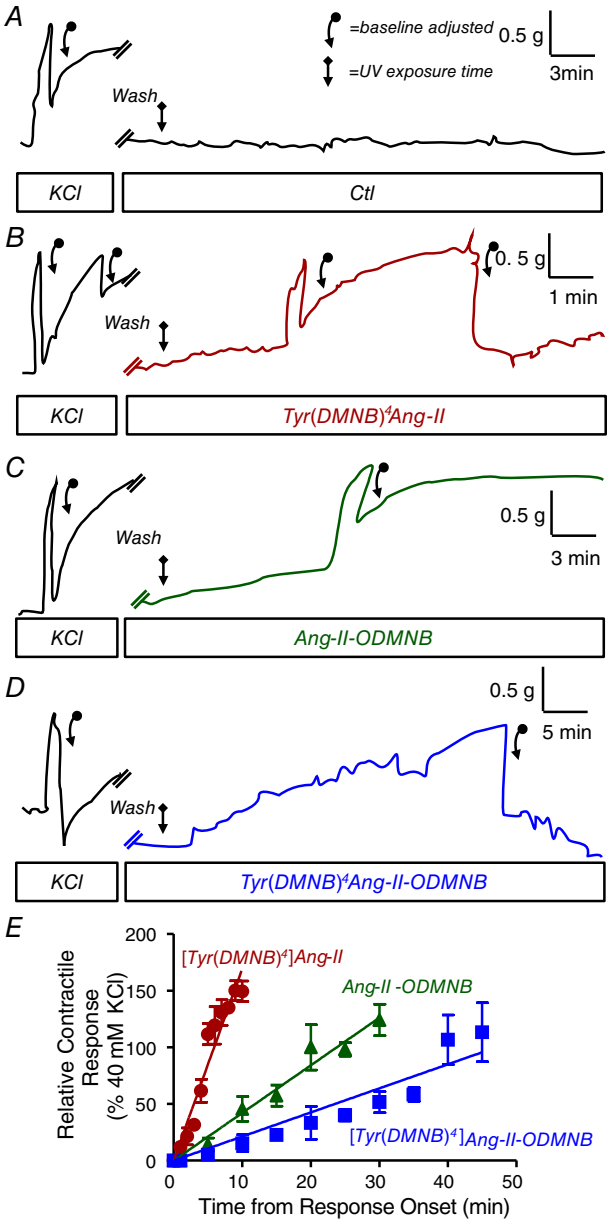

Figure 4. Contractile responses of rat thoracic aortic rings after photolysis of various analogues
Isometric aortic tension recording was obtained with a curvilinear pen recorder after a 15 min incubation in the presence of caged analogues (10^{-8} M) followed by *in situ* photolysis with 30-W UV-lamp. *A*, control. *B*, [Tyr(DMNB)^4]Ang-II. *C*, Ang-II-ODMNB. *D*, [Tyr(DMNB)^4]Ang-II-DMNB. *E*, overall results as a percentage of contractile response induced by 40 mM KCl. Data are shown as the mean ± SEM ($n = 4$ independent preparations from each of 4 animals per group).

Photolysis of [Tyr(DMNB)^4]Ang-II activates AT2R-mediated cGMP signalling

We then proceeded to examine the AT2-R-mediated biological activity of extracellular Ang-II photoreleased from caged analogues. AT2R-dependent cardiac-vessel vasodilatation is mediated by the NO/cGMP pathway (Tsutsumi *et al.* 1999). Therefore, we examined the effects of extracellular [Tyr(DMNB)^4]Ang-II and Ang-II on AT2R activation by measuring cGMP levels using an immunosorbent assay (Thermo Scientific, Waltham, MA, USA) in HEK 293 cells transiently transfected with AT2R. cGMP production in Ang-II-treated cells (10 nM, 45 min) was 2-fold greater than vehicle-treated cells (3.63 ± 0.43 pmol mg^{-1} protein *versus* 1.80 ± 0.22 pmol mg^{-1} protein) (Fig. 6). At the same concentration, [Tyr(DMNB)^4]Ang-II had no effect on the cGMP levels (2.24 ± 0.04 pmol mg^{-1} protein *versus* 2.17 ± 0.24 pmol mg^{-1} protein for cells exposed to UV-light alone). Upon uncaging by UV-irradiation, [Tyr(DMNB)^4]Ang-II (10 nM) increased the cellular cGMP content by 2-fold (4.51 ± 0.33 pmol mg^{-1} protein *versus* 2.17 ± 0.24 pmol mg^{-1} protein for cells exposed to UV-light alone). The effects of both Ang-II and irradiated [Tyr(DMNB)^4]Ang-II were abolished by preincubation with the AT2R-selective antagonist, PD 123319. Similarly, preincubating HEK 293 cells with the non-selective NO synthase inhibitor L-NAME markedly attenuated the increase in cGMP induced by both Ang-II and irradiated [Tyr(DMNB)^4]Ang-II. Hence, [Tyr(DMNB)^4]Ang-II (10 nM) alone is unable to activate AT2R but, upon photolysis, it shows strong AT2R-mediated activity.

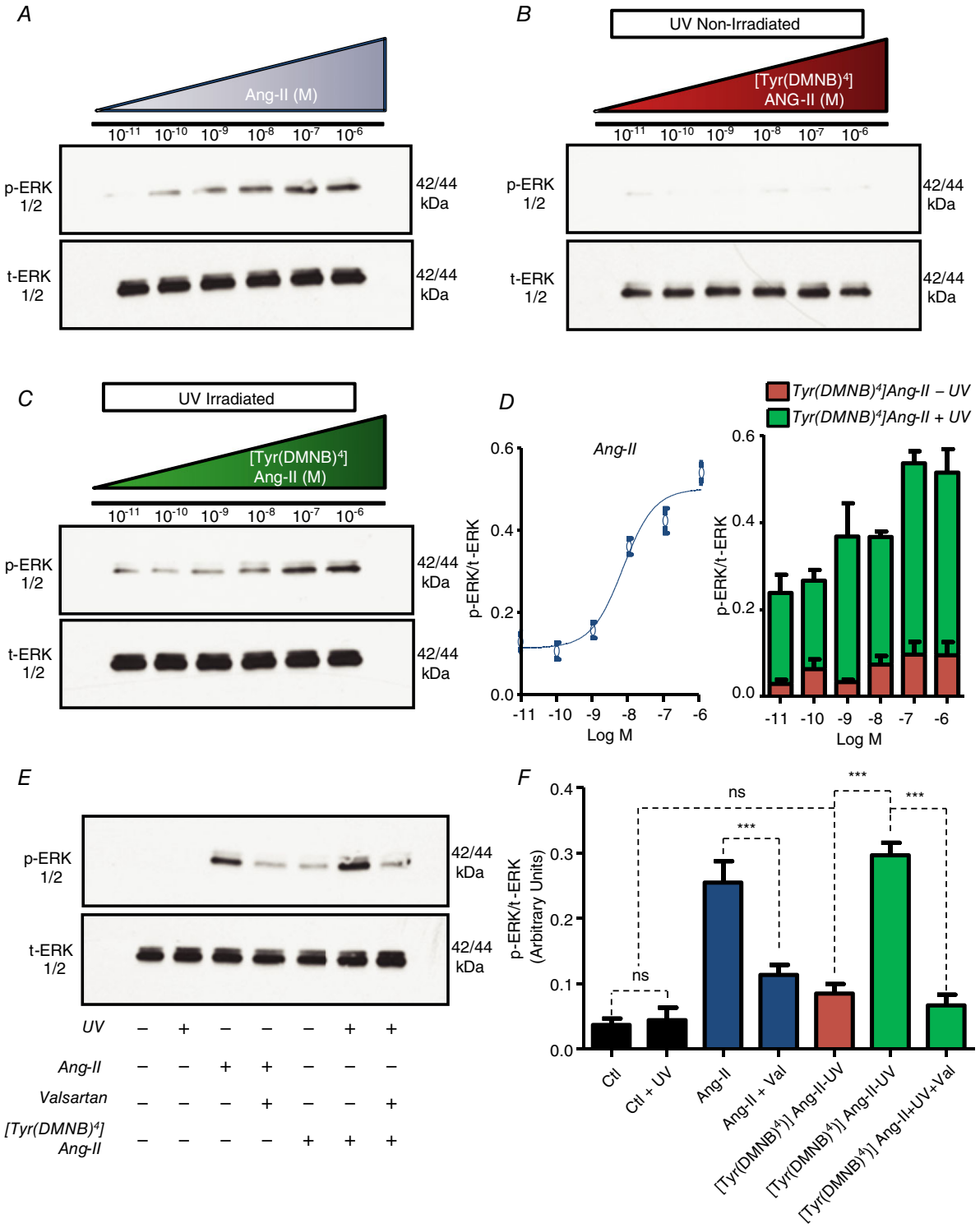

Figure 5. AT1R-dependent ERK-phosphorylation after photolysis of [Tyr(DMNB)^4]Ang-II
Effects of (*A*) Ang-II, (*B*) [Tyr(DMNB)^4]Ang-II and (*C*) UV-irradiated [Tyr(DMNB)^4]Ang-II on serum starved HEK 293 cells transfected with AT1R. Phosphorylated ERK1/2 (p-ERK) and total ERK1/2 (ERK) immunoreactivity was determined on cell-lysates. *D*, p-ERK immunoreactivity normalized to total ERK immunoreactivity (mean ± SEM). *E*, p-ERK and ERK immunoreactivity in AT1R-transfected HEK 293 cells treated with vehicle, in the presence or absence of 10 nM Ang-II or [Tyr(DMNB)^4]Ang-II (cAng-II), or valsartan (Val; 1 μM, 30 min) with or without UV-irradiation (1 min). *F*, mean ± SEM data corresponding to the experiment in (*E*) (n = 3 per concentration). $^{**}P < 0.01$, $^{***}P < 0.001$, ns, non-significant.

Cell permeability of [Tyr(DMNB)^4]Ang-II

To test the ability of [Tyr(DMNB)^4]Ang-II to cross the plasma membrane, we synthesized fluorescein-labelled derivatives of caged (fluorescein-[Ahx^0,Tyr(DMNB)^4]Ang-II) and uncaged (fluorescein-[Ahx^0]Ang-II) Ang-II. The uptake of Ang-II and [Tyr(DMNB)^4]Ang-II was compared with that of fluorescein-[Ahx^0]TAT(48–60), a cell-permeant peptide derived from the HIV transactivating regulatory protein TAT, and fluorescein-[Ahx^0]PACAP(28–38), a highly basic segment of pituitary adenylate cyclase-activating polypeptide previously characterized as having no cell-penetrating properties (Doan *et al.* 2012). Non-transfected HEK 293 cells were employed to minimize receptor-mediated endocytosis of Ang-II. Cells were treated with either fluorescein-[Ahx^0]Ang-II, fluorescein-[Ahx^0,Tyr(DMNB)^4]Ang-II, fluorescein-[Ahx^0]PACAP (28–38) or fluorescein-[Ahx^0]TAT(48–60) and the cellular uptake of the fluorescent peptides was analysed by both confocal fluorescence microscopy and flow cytometry (Fig. 7*A* and *B*). Cell Mask orange and DRAQ5 (a DNA-binding dye) were used to delineate the plasma membrane and nucleus, respectively. After acidic washes to remove peptides non-specifically bound to the extracellular surface, images of cellular fluorescence were acquired with a confocal microscope. Fluorescein-[Ahx^0]TAT(48–60) (2936 ± 410) produced a clear intracellular fluorescence signal, whereas almost no intracellular fluorescence was observed with fluorescein-[Ahx^0]PACAP(28–38) (186 ± 61). Overall, we observed significantly greater intracellular fluorescence intensity with fluorescein-[Ahx^0,Tyr(DMNB)^4]Ang-II (3475 ± 338) than with fluorescein-[Ahx^0]Ang-II (726 ± 74) (Fig. 7*C*). Further analysis with flow cytometry revealed that cells preincubated with fluorescein-[Ahx^0,Tyr(DMNB)^4]Ang-II displayed a much greater mean fluorescence signal (77 ± 2) than with fluorescein-[Ahx^0]Ang-II (24 ± 6) and even greater than the cell-permeant standard fluorescein-[Ahx^0]TAT(48–60) (60 ± 3) (Fig. 7*D*). Thus, Tyr(DMNB)^4]Ang-II is a potent cell-penetrating peptide that permits (i) delivery of a caged Ang-II analogue into intact live cells and (ii) spatial and temporal control of ligand release.

Photolysis of [Tyr(DMNB)^4]Ang-II inside cardiac cells increases nuclear calcium, 18S rRNA and NF-κB mRNA levels

Nuclear Ca^{2+} regulates essential cellular processes, including transcription, growth and apoptosis. Ang-II is a potent promoter of Ca^{2+} release but, so far, tools have been lacking to discriminate the contribution from organelle-localized *versus* cell-surface ATRs. Both AT1R and AT2R are expressed on nuclei of numerous cell types, including cardiomyocytes (Tadevosyan *et al.* 2012). Here, using live-cell confocal fluorescence microscopy, we examined the effect of intracellular [Tyr(DMNB)^4]Ang-II photolysis on nucleoplasmic Ca^{2+} ($[Ca^{2+}]_n$) and cytoplasmic Ca^{2+} ($[Ca^{2+}]_c$) in adult canine cardiomyocytes (Fig. 8*A–C*). Changes in $[Ca^{2+}]_n$ and $[Ca^{2+}]_c$ were visualized using the cell-permeant Ca^{2+} dye Fluo-4 AM. After exposure to 20 nM [Tyr(DMNB)^4]Ang-II, cells were thrice-washed to ensure removal of the extracellular moiety.

Photolysis of [Tyr(DMNB)^4]Ang-II caused a significant increase in $[Ca^{2+}]_n$ whereas non-photolysed [Tyr(DMNB)^4]Ang-II did not (Fig. 8*A* and *B*). To ensure that the photo-activated compound does not act via diffusion out of the cell followed by surface-receptor interaction, cells loaded with [Tyr(DMNB)^4]Ang-II

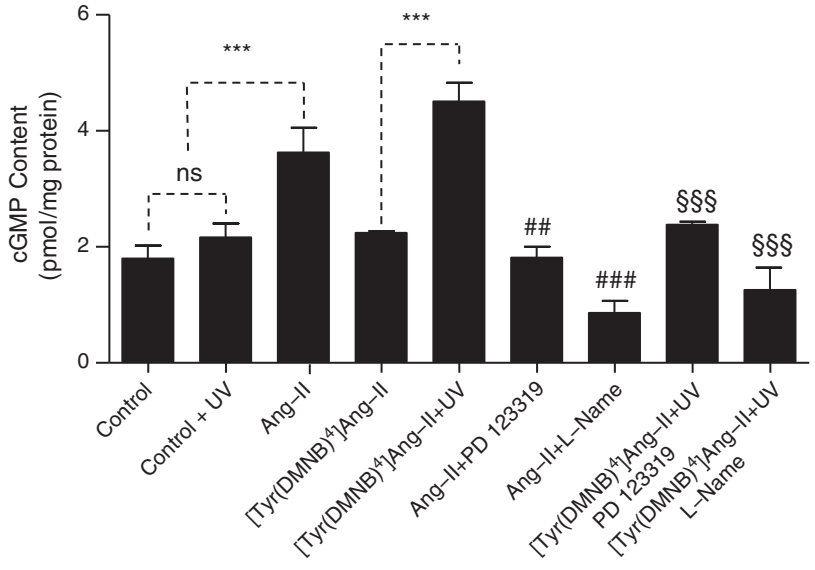

Figure 6. AT2R-dependent cGMP production after photolysis of [Tyr(DMNB)^4]Ang-II
cGMP was measured in serum-starved HEK 293 cells transfected with AT2R after incubation with vehicle (control), Ang-II (10 nM) or [Tyr(DMNB)^4]Ang-II, 10 nM) in the presence of PD123319 (PD, 1 μM), L-NAME (1 mM) and UV-irradiation, as indicated. Data are shown as the mean ± SEM ($n = 3$ per condition). ***$P < 0.001$, ##$P < 0.01$ or ###$P < 0.001$ *versus* Ang-II, §§§$P < 0.001$ *versus* [Tyr(DMNB)^4]Ang-II. ns, non-significant.

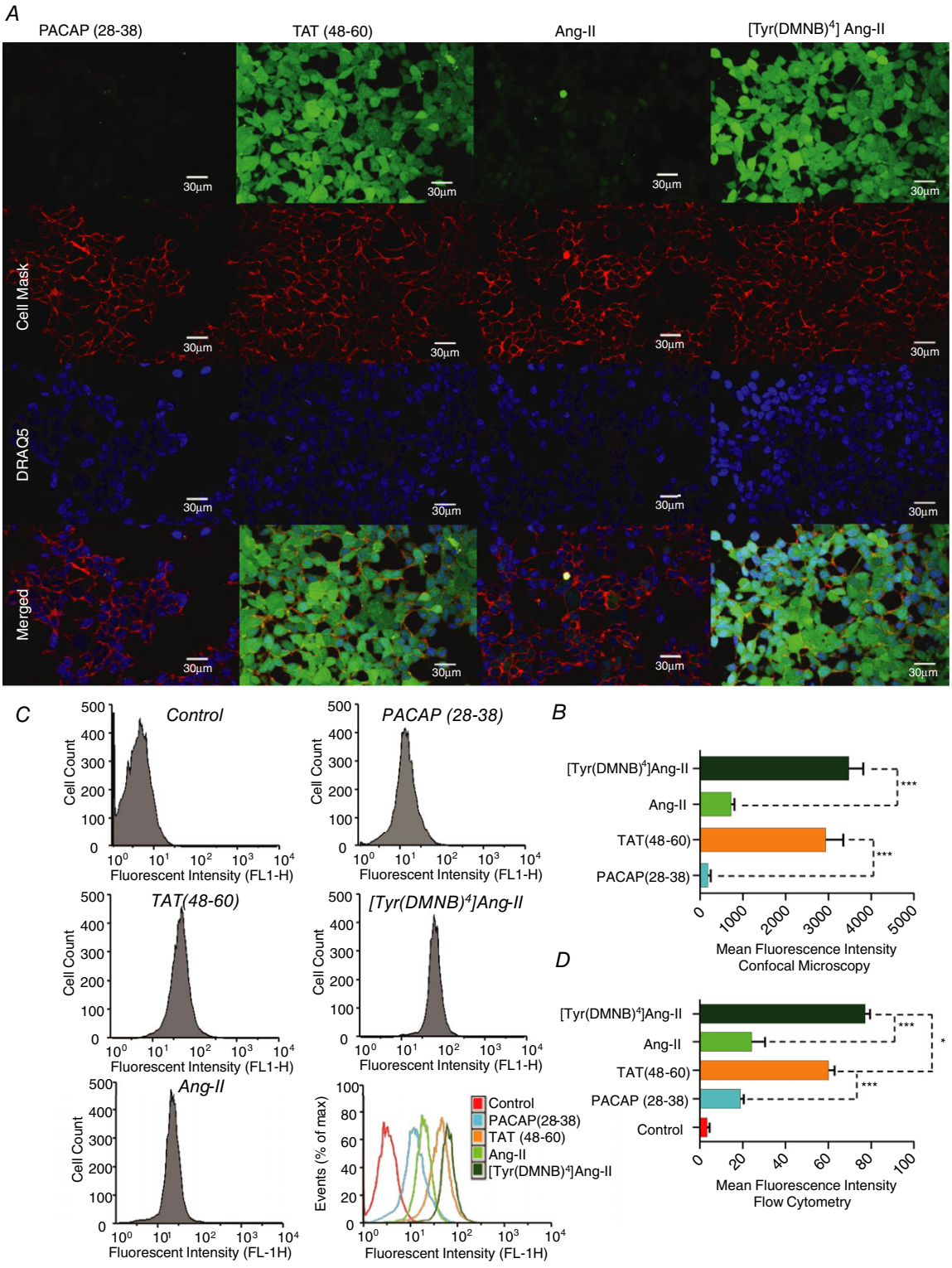

Figure 7. Cellular uptake of fluorescein-[Ahx^0,Tyr(DMNB)^4]Ang-II
A, intracellular distribution of fluorescein-[Ahx^0]Ang-II, fluorescein-[Ahx^0,Tyr(DMNB)^4]Ang-II, fluorescein-[Ahx^0]PACAP(28–38) and fluorescein-[Ahx^0]TAT(48–60) upon confocal microscopy in live non-permeabilized HEK 293 cells. Cell Mask and DRAQ5 were used to delineate the plasma membrane and nuclei, respectively. *B*, intracellular fluorescence intensity (mean ± SEM; ***$P < 0.001$). *C*, representative uptake efficiency of fluorescein-conjugated PACAP(28–38), TAT(48–60), Ang-II and [Tyr(DMNB)^4]Ang-II in HEK 293 cells upon flow cytometry; quantified (*D*) with fluorescence-activated cell sorting analysis software FlowJo (mean ± SEM; $n = 3$ per condition; *$P < 0.05$, ***$P < 0.001$).

were pre-treated for 20 min and photolysed in the presence of 1 μM valsartan. Valsartan did not reduce the magnitude of the increase in $[Ca^{2+}]_n$ at 400 s post-photolysis of [Tyr(DMNB)^4]Ang-II, but the increase in $[Ca^{2+}]_n$ was more rapid in the presence of valsartan. Hence, after photolysis, Ang-II does not increase $[Ca^{2+}]_n$ by leaving the cell and acting on cell-surface receptors; however, there may be cross-talk between cell surface and nuclear ATRs. Cells exposed to 100 μM 2-aminoethoxydiphenylborate (2-APB) to block IP_3 receptors (the principal angiotensin-dependent nuclear Ca^{2+}-entry pathway (Tadevosyan *et al.* 2010)) displayed a significant decrease in $[Ca^{2+}]_n$ accumulation after photolysis. Sham-loaded cardiomyocytes (i.e. without [Tyr(DMNB)^4]Ang-II in the loading buffer) displayed no change in $[Ca^{2+}]_n$ in response to UV-irradiation (Fig. 8*B*). Extracellular application of 20 nM Ang-II caused a slow and limited increase in $[Ca^{2+}]_n$, relative to that induced by intracellular photolysis of [Tyr(DMNB)^4]Ang-II, and this effect was abolished when cells were pretreated with 1 μM valsartan. The changes in $[Ca^{2+}]_c$ in response to photolysis of [Tyr(DMNB)^4]Ang-II were generally similar to that of $[Ca^{2+}]_n$, but the increases in fluorescence intensity were smaller for $[Ca^{2+}]_c$ (Fig. 8*B* and *C*). To compare directly the $[Ca^{2+}]_n$ response with the $[Ca^{2+}]_c$ response, we normalized each to their respective baseline values (Fig. 8*D*). The $[Ca^{2+}]_n$ response occurred with or before the $[Ca^{2+}]_c$ response, making it improbable that the $[Ca^{2+}]_n$ increases are secondary to the change in $[Ca^{2+}]_c$. Figure 8*E* indicates the mean response in each group by showing mean baseline ($t = 10$ s) *versus* post-photolysis ($t = 400$ s) values.

We have shown previously that Ang-II increases the transcription of rRNA and NF-κB mRNA in nuclei isolated from rat adult cardiomyocytes (Tadevosyan *et al.* 2010). Similarly, photolysis of [Tyr(DMNB)^4]Ang-II (cAng-II) increased 18S rRNA and NF-κB mRNA, compared to the more slowly photolysed Ang-II-ODMNB, in intact cardiomyocytes (Fig. 9). Therefore, selective activation of intracellular ATRs in cardiomyocytes increases $[Ca^{2+}]_n$ and regulates gene transcription.

Discussion

The intracrine RAS has been suggested to control intracellular Ca^{2+}-fluxes, generation of reactive oxygen species, junctional conductance, cell volume, chromatin solubility, gene transcription and post-translational histone modifications (Re & Cook, 2011). The presence of functional Ang-II receptors on the nuclear membrane, along with the nuclear localization of carboxy-terminal sequence of the AT1R (Lee *et al.* 2004), provided additional support for the idea that classical receptor signalling occurs on intracellular membranes (Morinelli *et al.* 2007). To further examine this concept and to develop a tool for exploring it, we synthesized novel caged, cell-permeant Ang-II analogues, with [Tyr(DMNB)^4]Ang-II being the most effective, allowing spatio-temporal control of ATR activation within intact cells. Furthermore, we have shown that photolysis of [Tyr(DMNB)^4]Ang-II inside intact cardiomyocytes increases $[Ca^{2+}]_n$, as well as 18S rRNA and NF-κB mRNA levels.

A variety of approaches, each with its own challenges and technical limitations, have been applied *in vitro* and *in vivo* to study the role of the intracrine RAS. In a previous study, transgenic mice were bred that expressed a construct comprising Ang-II fused in-frame to the enhanced cyan fluorescent protein (ECFP), linked by a small spacer arm, under the control of the mouse metallothionein promoter (Redding *et al.* 2010). This construct was developed in a manner that ensures that ECFP-Ang-II is synthesized but retained intracellularly because it was unable to access the secretory pathway. Although this transgene resulted in changed diastolic and systolic blood pressure, as well as thrombotic renal microangiopathy, its expression was ubiquitous rather than intracellularly targeted. Similarly, another study used the sgtl2 gene promoter to selectively drive expression of ECFP-Ang-II in proximal renal tubules; however, this construct was delivered using an adenovirus and, hence, the effect was transient (Li *et al.* 2011). Furthermore, *in vivo* delivery to other organs might have been hampered by host immune responses. There have been several reports in which liposomes were used to deliver hormones intracellularly. It was demonstrated that liposomal delivery of Ang-II into A7r5 cells induced cell growth through activation of the phosphoinositide 3-kinase and MAPK/ERK pathways (Filipeanu *et al.* 2001). However, during liposomal delivery only a small fraction (7.2 $\pm$ 0.2%) of the administered Ang-II was actually taken up into target cells. Additional disadvantages of the liposomal delivery strategy include an inability to target the cargo to a specific cell type, biological instability as a result of the amphiphilic character of liposomes, interactions with lipoproteins, and interactions with common degradation pathways. Microinjection was used to introduce Ang-II into ventricular cardiomyocytes and an increased inward Ca^{2+} current (I_{Ca}) and altered myocardial contractility were observed (De Mello, 1998). Similarly, it was reported that microinjection of Ang-II into vascular smooth muscle cells induced a rise in $[Ca^{2+}]$ within the injected cell and also in adjacent cells (Haller *et al.* 1996). It was concluded that Ang-II stimulated a cluster of vascular smooth muscle cells via release of diffusible intracellular second messengers from the injected cell. Nevertheless, the possibility that observed effects were because of outflow of the peptide that eventually activated neighbouring cell-surface receptors could not be excluded. Moreover, although microinjection provides a way to introduce an agonist (or antagonist) into a cell, it can only be applied realistically to single cell

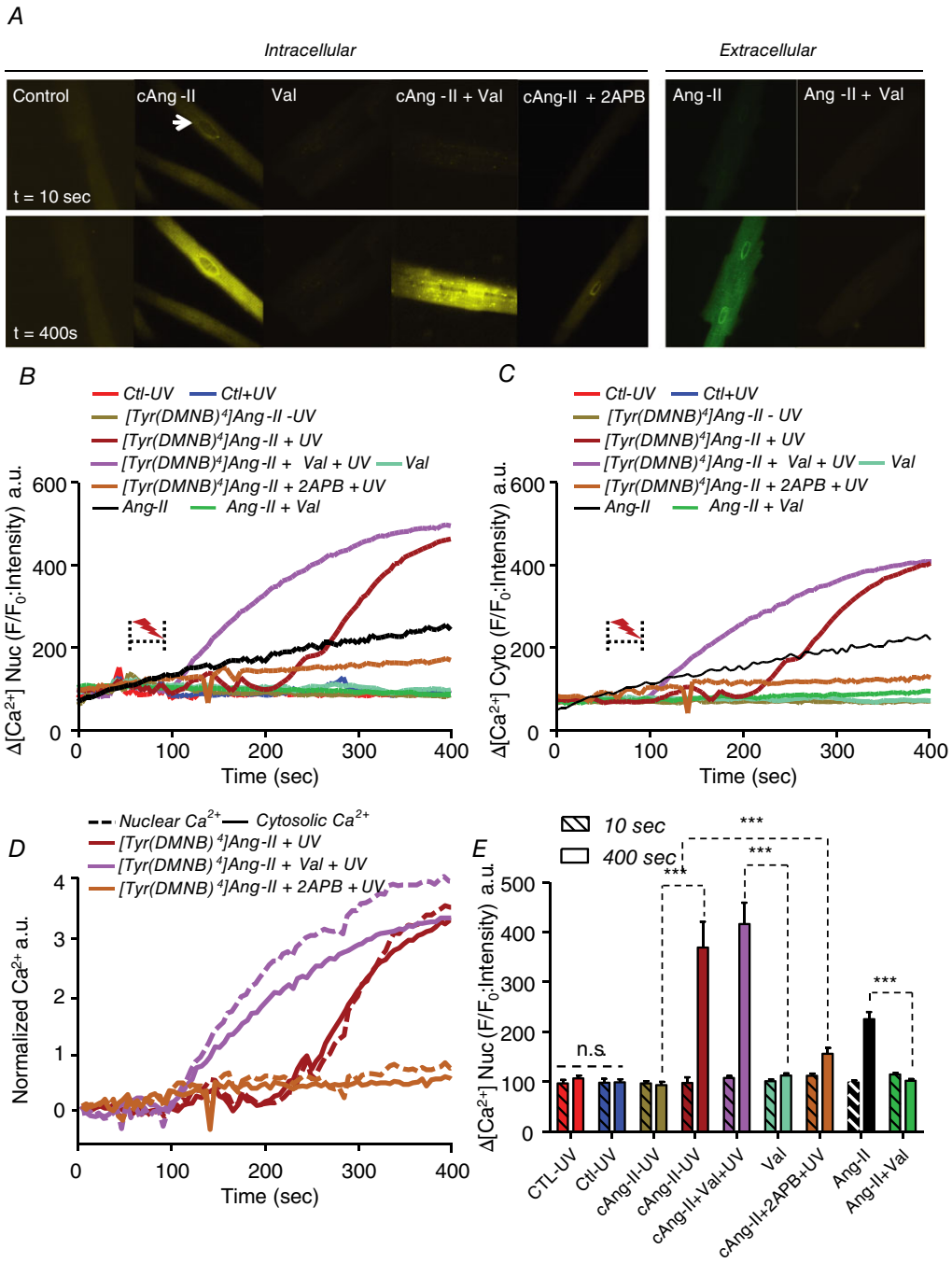

Figure 8. Response of nucleoplasmic and cytosolic [Ca^{2+}] to photolysis of intracellular [Tyr(DMNB)^4]Ang-II

A, nucleoplasmic and cytosolic [Ca^{2+}] recorded in canine cardiomyocytes before (t = 10 s) and after (t = 400 s) photolysis in cells loaded with vehicle (control), 20 nM [Tyr(DMNB)^4]Ang-II (cAng-II), 20 nM cAng-II + 1 μM valsartan, 20 nM cAng-II + 100 μM 2-APB, 1 μM valsartan alone or extracellularly administered 20 nM Ang-II with or without 1 μM valsartan. Photolysis was induced by a pulse of UV-light (2–5 s, 70 μW) from a 405 nm/30 mW diode. Nucleoplasmic (*B*) and cytosolic (*C*) [Ca^{2+}] recorded in ventricular cardiomyocytes before and after photolysis in cells preincubated with [Tyr(DMNB)^4]Ang-II, vehicle (Ctl), valsartan, 2-APB along with non-photolysed [Tyr(DMNB)^4]Ang-II or vehicle. Dotted bracket, UV-irradiation. DRAQ5 fluorescence was used to select the area corresponding to the nucleoplasm. Signals are presented as background-subtracted normalized fluorescence (%F/F_0), where F is the fluorescence intensity and F_0 is the resting fluorescence in the same cell prior to photolysis. *D*, [Ca^{2+}] fluorescence in the nucleus and cytosol normalized to respective baseline (t = 10 s) values. Nuclear changes are indicated by dashed lines and cytosolic by continuous lines. *E*, for each condition (n = 8–12 cells), mean nuclear Fluo-4 fluorescence at baseline (t = 10 s; hatched bars) or after stimulation (t = 400 s) was quantified. Data are shown as the mean ± SEM; ***$P < 0.000$. ns, non-significant.

experiments and, therefore, similar to liposomal delivery, it is not amenable to biochemical analysis of intracrine effects.

The development of caged, cell-permeant Ang-II analogues will permit the study of the molecular pharmacology and physiological function of endogenous ATRs in a broad range of primary cells and possibly *ex vivo* tissue preparations. Insights into the structural interactions involving Ang-II and its receptors guided the design of caged peptide analogues to selectively interfere with receptor binding and activation (Chaulk & MacMillan, 1998; Monroe *et al.* 1999; Ando *et al.* 2001). The photolabile DMNB exhibits maximal absorption in the near UV-range ($\lambda = 365$ nm), excellent solubility in aqueous solution, and is compatible with sensitive biological preparations. In the present study, DMNB was introduced at the phenolic hydroxyl group of Tyr^4 and/or at the carboxyl function of Phe^8 of Ang-II (Fig. 1*A–D*). The addition of DMNB enhanced the lipophilicity of Ang-II, allowing [Tyr(DMNB)^4]AngII to cross plasma membranes efficiently, at the same time as remaining water soluble. Cell permeability was so effective that the intracellular accumulation of [Tyr(DMNB)^4]AngII was greater than that of a potent cell-penetrating peptide derived from the HIV-1 trans-activating protein, TAT (Fig. 7). All three synthetic caged analogues, namely [Tyr(DMNB)^4]Ang-II, Ang-II-ODMNB and [Tyr(DMNB)^4]Ang-II-ODMNB), showed greatly decreased ability to bind and activate ATRs in the absence of photolysis. [Tyr(DMNB)^4]Ang-II was the best suited for live-cell studies because of its rapid photolysis kinetics. This characteristic allows the study of events occurring on a rapid time scale and minimizes exposure of target-cells to UV-irradiation. Rapid photolysis also permits evaluation of the effects of acute ligand application in either single cells or a cell population, an experimental condition that cannot be achieved with liposomes or microinjection. The temporal and spatial control of Ang-II release upon UV-irradiation provides a versatile tool for studying the functional and molecular pharmacology of intracrine Ang-II signalling. We examined the effects of [Tyr(DMNB)^4]Ang-II in isolated tissue preparations, cultured HEK 293 cells and isolated adult cardiomyocytes. Studies in these systems confirmed the reduction in intrinsic affinity and activity of [Tyr(DMNB)^4]Ang-II, compared to Ang-II, and its capacity to demonstrate substantial pharmacological potency and efficacy upon photolysis.

Although we previously demonstrated the mobilization of nuclear Ca^{2+} (which could be blocked by 2-APB) and *de novo* mRNA synthesis upon exposure to Ang-II in isolated nuclei (Tadevosyan *et al.* 2010), the physiological significance remained unclear in the absence of convincing evidence in an intact cell system. Here, we used photorelease of Ang-II from a caged analogue to show intracellular Ang-II dependent mobilization of nuclear Ca^{2+}, along with *de novo* RNA synthesis, in intact cardiomyocytes. This effect was suppressed by 2-APB, potentially implicating IP_3 receptors, whereas extracellular valsartan did not alter the response. Thus, the caged compound allowed us for the first time to show convincingly that intracellular Ang-II increases nucleoplasmic and cytosolic [Ca^{2+}] in intact cardiomyocytes, with pharmacological evidence suggesting that this action is independent of extracellular receptors and that IP_3 receptors might play an important role. Further work is needed to clarify the precise mechanisms underlying [Ca^{2+}] changes in

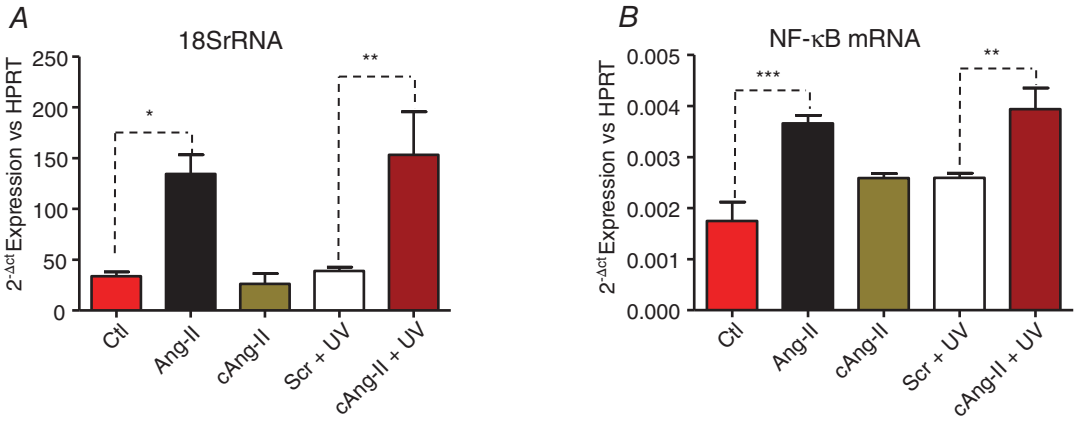

Figure 9. Photolysis of intracellular [Tyr(DMNB)4]Ang-II regulates transcription
18S rRNA (A) and NF-κB mRNA (B) were quantified by quantitative PCR. A stimulation-control (scr) condition was performed where cardiomyocytes were loaded with a slowly-photolysing Ang-II analogue, Ang-II-ODMNB. Myocytes were incubated with [Tyr(DMNB)^4]Ang-II or Ang-II-ODMNB (10 nM) for 30 min at room temperature. After incubation, cells were washed, placed on ice and exposed to a UV-lamp (30 W) for 1 min. In addition, cells were examined after treatment with buffer (Ctl) or extracellular Ang-II (Ang-II; 10 nM). Cells were then incubated at 37°C for 4 h prior to RNA extraction. Data are shown as the mean ± SEM; $^*P < 0.05$, $^{**}P < 0.01$, $^{***}P < 0.0001$.

various subcellular compartments produced by intracellular Ang-II. In principle, the probes developed in the present study could be used to investigate the role of intracellular Ang-II not only in cardiomyocytes, but also in any cell-type.

In summary, we have revealed the effectiveness of incorporating a photosensitive DMNB blocking group on the tyrosine-4 side chain of Ang-II in creating a cell-permeant, photo-activable Ang-II analogue. The corresponding caged Ang-II analogue, [Tyr(DMNB)^4]Ang-II, was stable, pharmacologically inactive within the required concentration range, rapidly released upon exposure to UV-light, and rapidly released active Ang-II upon photolysis. Furthermore, when loaded into live cells, uncaging [Tyr(DMNB)^4]Ang-II with a localized pulse from a UV-laser produces spatial and temporal release of Ang-II that, unlike other means of delivery, allows both pharmacological and functional studies of the intracrine Ang-II system in both primary and cultured cells.

References

Ando H, Furuta T, Tsien RY & Okamoto H (2001). Photo-mediated gene activation using caged RNA/DNA in zebrafish embryos. *Nat Genet* **28**, 317–325.

Aumelas A, Sakarellos C, Lintner K, Fermandjian S, Khosla MC, Smeby RR & Bumpus FM (1985). Studies on angiotensin II and analogs: impact of substitution in position 8 on conformation and activity. *Proc Natl Acad Sci U S A* **82**, 1881–1885.

Bosnyak S, Jones ES, Christopoulos A, Aguilar MI, Thomas WG & Widdop RE (2011). Relative affinity of angiotensin peptides and novel ligands at AT1 and AT2 receptors. *Clin Sci (Lond)* **121**, 297–303.

Bourgault S, Letourneau M & Fournier A (2005). Development and pharmacological characterization of "caged" urotensin II analogs. *Peptides* **26**, 1475–1480.

Bourgault S, Letourneau M & Fournier A (2007). Development of photolabile caged analogs of endothelin-1. *Peptides* **28**, 1074–1082.

Bovy PR, O'Neal JM, Olins GM, Patton DR, McMahon EG, Palomo M, Koepke JP, Salles KS, Trapani AJ, Smits GJ, McGraw DE & Hutton WC (1990). Structure-activity relationships for the carboxy-terminus truncated analogues of angiotension II, a new class of angiotensin II antagonists. *J Med Chem* **33**, 1477–1482.

Chaulk SG & MacMillan AM (1998). Caged RNA: photo-control of a ribozyme reaction. *Nucleic Acids Res* **26**, 3173–3178.

Cook JL, Mills SJ, Naquin R, Alam J & Re RN (2006). Nuclear accumulation of the AT1 receptor in a rat vascular smooth muscle cell line: effects upon signal transduction and cellular proliferation. *J Mol Cell Cardiol* **40**, 696–707.

Dawson K, Wu CT, Qi XY & Nattel S (2012). Congestive heart failure effects on atrial fibroblast phenotype: differences between freshly-isolated and cultured cells. *PLoS One* **7**, e52032.

DeMello WC (1998). Intracellular angiotensin II regulates the inward calcium current in cardiac myocytes. *Hypertension* **32**, 976–982.

Doan ND, Letourneau M, Vaudry D, Doucet N, Folch B, Vaudry H, Fournier A & Chatenet D (2012). Design and characterization of novel cell-penetrating peptides from pituitary adenylate cyclase-activating polypeptide. *J Control Release* **163**, 256–265.

Filipeanu CM, Henning RH, de Zeeuw D & Nelemans A (2001). Intracellular Angiotensin II and cell growth of vascular smooth muscle cells. *Br J Pharmacol* **132**, 1590–1596.

Frustaci A, Kajstura J, Chimenti C, Jakoniuk I, Leri A, Maseri A, Nadal-Ginard B & Anversa P (2000). Myocardial cell death in human diabetes. *Circ Res* **87**, 1123–1132.

Ghosh M, Song X, Mouneimne G, Sidani M, Lawrence DS & Condeelis JS (2004). Cofilin promotes actin polymerization and defines the direction of cell motility. *Science* **304**, 743–746.

Haller H, Lindschau C, Erdmann B, Quass P & Luft FC (1996). Effects of intracellular angiotensin II in vascular smooth muscle cells. *Circ Res* **79**, 765–772.

Haller H, Lindschau C, Quass P & Luft FC (1999). Intracellular actions of angiotensin II in vascular smooth muscle cells. *J Am Soc Nephrol* **10**(Suppl 11), S75–83.

Jullian M, Hernandez A, Maurras A, Puget K, Amblard M, Martinez J & Subra G (2009). N-terminus FITC labeling of peptides on solid support: the truth behind the spacer. *Tetrahedron Lett* **50**, 260–263.

Kobori H, Nangaku M, Navar LG & Nishiyama A (2007). The intrarenal renin-angiotensin system: from physiology to the pathobiology of hypertension and kidney disease. *Pharmacol Rev* **59**, 251–287.

Lang CC & Struthers AD (2013). Targeting the renin-angiotensin-aldosterone system in heart failure. *Nat Rev Cardiol* **10**, 125–134.

Lee DK, Lanca AJ, Cheng R, Nguyen T, Ji XD, Gobeil F, Jr., Chemtob S, George SR & O'Dowd BF (2004). Agonist-independent nuclear localization of the Apelin, angiotensin AT1, and bradykinin B2 receptors. *J Biol Chem* **279**, 7901–7908.

Li XC, Cook JL, Rubera I, Tauc M, Zhang F & Zhuo JL (2011). Intrarenal transfer of an intracellular fluorescent fusion of angiotensin II selectively in proximal tubules increases blood pressure in rats and mice. *Am J Physiol Renal Physiol* **300**, F1076–F1088.

Li W, Llopis J, Whitney M, Zlokarnik G & Tsien RY (1998). Cell-permeant caged $InsP_3$ ester shows that Ca^{2+} spike frequency can optimize gene expression. *Nature* **392**, 936–941.

McCray JA, Herbette L, Kihara T & Trentham DR (1980). A new approach to time-resolved studies of ATP-requiring biological systems; laser flash photolysis of caged ATP. *Proc Natl Acad Sci U S A* **77**, 7237–7241.

Merlen C, Farhat N, Luo X, Chatenet D, Tadevosyan A, Villeneuve LR, Gillis MA, Nattel S, Thorin E, Fournier A & Allen BG (2013). Intracrine endothelin signaling evokes IP3-dependent increases in nucleoplasmic Ca in adult cardiac myocytes. *J Mol Cell Cardiol* **62**, 189–202.

Monroe WT, McQuain MM, Chang MS, Alexander JS & Haselton FR (1999). Targeting expression with light using caged DNA. *J Biol Chem* **274**, 20895–20900.

Morinelli TA, Raymond JR, Baldys A, Yang Q, Lee MH, Luttrell L & Ullian ME (2007). Identification of a putative nuclear localization sequence within ANG II AT_{1A} receptor associated with nuclear activation. *Am J Physiol Cell Physiol* **292**, C1398–C1408.

Muralidharan S, Maher GM, Boyle WA & Nerbonne JM (1993). "Caged" phenylephrine: development and application to probe the mechanism of alpha-receptor-mediated vasoconstriction. *Proc Natl Acad Sci U S A* **90**, 5199–5203.

Muralidharan S & Nerbonne JM (1995). Photolabile "caged" adrenergic receptor agonists and related model compounds. *J Photochem Photobiol B* **27**, 123–137.

Noda K, Saad Y & Karnik SS (1995). Interaction of Phe^8 of angiotensin II with Lys^{199} and His^{256} of AT_1 receptor in agonist activation. *J Biol Chem* **270**, 28511–28514.

Re RN & Cook JL (2011). Noncanonical intracrine action. *J Am Soc Hypertens* **5**, 435–448.

Redding KM, Chen BL, Singh A, Re RN, Navar LG, Seth DM, Sigmund CD, Tang WW & Cook JL (2010). Transgenic mice expressing an intracellular fluorescent fusion of angiotensin II demonstrate renal thrombotic microangiopathy and elevated blood pressure. *Am J Physiol Heart Circ Physiol* **298**, H1807–H1818.

Robertson AL Jr & Khairallah PA (1971). Angiotensin II: rapid localization in nuclei of smooth and cardiac muscle. *Science* **172**, 1138–1139.

Samanen J, Cash T, Narindray D, Brandeis E, Yellin T & Regoli D (1989). The role of position 4 in angiotensin II antagonism: a structure-activity study. *J Med Chem* **32**, 1366–1370.

Schlichting I, Rapp G, John J, Wittinghofer A, Pai EF & Goody RS (1989). Biochemical and crystallographic characterization of a complex of c-Ha-ras p21 and caged GTP with flash photolysis. *Proc Natl Acad Sci U S A* **86**, 7687–7690.

Schwab AJ, Barker F 3rd, Goresky CA & Pang KS (1990). Transfer of enalaprilat across rat liver cell membranes is barrier limited. *Am J PhysiolGastrointest Liver Physiol* **258**, G461–G475.

Singh VP, Le B, Bhat VB, Baker KM & Kumar R (2007). High-glucose-induced regulation of intracellular ANG II synthesis and nuclear redistribution in cardiac myocytes. *Am J Physiol Heart Circ Physiol* **293**, H939–H948.

Singh VP, Le B, Khode R, Baker KM & Kumar R (2008). Intracellular angiotensin II production in diabetic rats is correlated with cardiomyocyte apoptosis, oxidative stress, and cardiac fibrosis. *Diabetes* **57**, 3297–3306.

Tadevosyan A, Allen BG & Nattel S (2015). Isolation and study of cardiac nuclei from canine myocardium and adult ventricular myocytes. *MethodsMol Biol* **1234**, 69–80.

Tadevosyan A, Maguy A, Villeneuve LR, Babin J, Bonnefoy A, Allen BG & Nattel S (2010). Nuclear-delimited angiotensin receptor-mediated signaling regulates cardiomyocyte gene expression. *J Biol Chem* **285**, 22338–22349.

Tadevosyan A, Vaniotis G, Allen BG, Hebert TE & Nattel S (2012). G protein-coupled receptor signalling in the cardiac nuclear membrane: evidence and possible roles in physiological and pathophysiological function. *J Physiol* **590**, 1313–1330.

Tertyshnikova S & Fein A (1998). Inhibition of inositol 1,4,5-trisphosphate-induced Ca^{2+} release by cAMP-dependent protein kinase in a living cell. *Proc Natl Acad Sci U S A* **95**, 1613–1617.

Tsutsumi Y, Matsubara H, Masaki H, Kurihara H, Murasawa S, Takai S, Miyazaki M, Nozawa Y, Ozono R, Nakagawa K, Miwa T, Kawada N, Mori Y, Shibasaki Y, Tanaka Y, Fujiyama S, Koyama Y, Fujiyama A, Takahashi H & Iwasaka T (1999). Angiotensin II type 2 receptor overexpression activates the vascular kinin system and causes vasodilation. *J Clin Invest* **104**, 925–935.

Vaniotis G, Glazkova I, Merlen C, Smith C, Villeneuve LR, Chatenet D, Therien M, Fournier A, Tadevosyan A, Trieu P, Nattel S, Hebert TE & Allen BG (2013). Regulation of cardiac nitric oxide signalling by nuclear beta-adrenergic and endothelin receptors. *J Mol Cell Cardiol* **62**, 58–68.

Wang SS & Augustine GJ (1995). Confocal imaging and local photolysis of caged compounds: dual probes of synaptic function. *Neuron* **15**, 755–760.

Yu H, Li J, Wu D, Qiu Z & Zhang Y (2010). Chemistry and biological applications of photo-labile organic molecules. *Chem Soc Rev* **39**, 464–473.

Zhang X, Wang G, Dupre DJ, Feng Y, Robitaille M, Lazartigues E, Feng YH, Hebert TE & Wu G (2009). Rab1 GTPase and dimerization in the cell surface expression of angiotensin II type 2 receptor. *J Pharmacol Exp Ther* **330**, 109–117.

Zimmerman B, Beautrait A, Aguila B, Charles R, Escher E, Claing A, Bouvier M & Laporte SA (2012). Differential beta-arrestin-dependent conformational signaling and cellular responses revealed by angiotensin analogs. *Sci Signal* **5**, ra33.

Additional information

Competing interests

None.

Author contributions

A.T., A.F., D.C., B.G.A. and S.N. participated in the conception of the study and the experimental design. A.T., M.L. and D.C. carried out the peptide synthesis, binding assays, and biochemical and physiological experiments. B.F. and N.D. performed the computer simulation experiments needed to design Ang-II analogues and plan their synthesis. A.M.M., D.P. and T.E.H participated in the purification and expression in HEK 293 cells of expression vectors encoding AT1R-Venus and AT2R-Venus. A.T. and L.R.V. performed and analysed immunohistochemical and calcium imaging experiments. A.T., B.G.A. and S.N. participated in the analysis and interpretation of data, as well as the drafting and revision of the manuscript. All authors

read and approved the final version of the manuscript submitted for publication.

Funding

The present study was supported by grants from the Canadian Institutes for Health Research (CIHR, 6957 and 68929), the Quebec Heart and Stroke Foundation, and the Fondation Leducq (ENAFRA Network, 07/CVD/03). A.T. was supported by an FRQS-RSCV/HSFQ doctoral scholarship. B.F. was supported by a postdoctoral fellowship from the 'Fondation universitaire Armand-Frappier de l'INRS' and a Banting Research Foundation grant.

Acknowledgements

The authors thank Nathalie L'Heureux and Chantal St-Cyr for providing technical assistance, Dr Feng Xiong for statistical analyses and France Thériault for secretarial help with the manuscript.